

Glaciations in response to climate variations preconditioned by evolving topography

Vivi Kathrine Pedersen¹ & David Lundbek Egholm²

Landscapes modified by glacial erosion show a distinct distribution of surface area with elevation^{1–3} (hypsometry). In particular, the height of these regions is influenced by climatic gradients controlling the altitude where glacial and periglacial processes are the most active, and as a result, surface area is focused just below the snowline altitude^{1–9}. Yet the effect of this distinct glacial hypsometric signature on glacial extent and therefore on continued glacial erosion has not previously been examined. Here we show how this topographic configuration influences the climatic sensitivity of Alpine glaciers, and how the development of a glacial hypsometric distribution influences the intensity of glaciations on timescales of more than a few glacial cycles. We find that the relationship between variations in climate and the resulting variation in areal extent of glaciation changes drastically with the degree of glacial modification in the landscape. First, in landscapes with novel glaciations, a nearly linear relationship between climate and glacial area exists. Second, in previously glaciated landscapes with extensive area at a similar elevation, highly nonlinear and rapid glacial expansions occur with minimal climate forcing, once the snowline reaches the hypsometric maximum. Our results also show that erosion associated with glaciations before the mid-Pleistocene transition at around 950,000 years ago probably preconditioned the landscape—producing glacial landforms and hypsometric maxima—such that ongoing cooling led to a significant change in glacial extent and erosion, resulting in more extensive glaciations and valley deepening in the late Pleistocene epoch. We thus provide a mechanism that explains previous observations from exposure dating¹⁰ and low-temperature thermochronology¹¹ in the European Alps, and suggest that there is a strong topographic control on the most recent Quaternary period glaciations.

It has long been recognized that topographic feedbacks between glacial erosion and glacial mass balance influence glaciations^{7,12–20}. For example, previous numerical studies have shown how glacial erosion can reduce the extent of subsequent glaciations under constant climate conditions by lowering of topography^{13,18}. However, the effect of a distinct glacial landscape hypsometry on glacial extent through several glacial cycles has not been considered explicitly, and limited work only has focused on transient effects in glacial extent resulting from glacial erosion processes modifying the topography^{13,16–20}.

Here we examine the response of mountain-range glaciations to the present topographic distribution for a varying climate using a numerical surface process model, including an ice-sheet model suitable for rugged mountain topography^{21–23} (see Methods Summary and Supplementary Information). Furthermore, in an additional experiment, we impose a climate forcing comparable with Quaternary climate records²⁴, to investigate possible feedbacks between climate, topography, glacial extent and glacial erosion that may have prevailed throughout the last two million years (Myr) of Earth's history.

The hypsometry of a landscape influences the mass balance of glaciers, because it dictates how much surface area is available for snow and ice accumulation when paired with a temperature–elevation distribution. Therefore, for a given variation in snowline altitude, the

change in glacier accumulation area is a nonlinear function of the topographic configuration. This nonlinearity becomes increasingly pronounced through the development of the distinct hypsometric maximum found worldwide below the present snowline altitude for glacially modified areas^{2,3} (see Supplementary Figs 1–5).

To illustrate this, we use our numerical approach for simulating glaciation of a catchment from Sierra Nevada, Spain, where limited glacial activity has occurred throughout the Quaternary²⁵, and of a catchment from the Bitterroot Range, USA, which has been significantly modified by glaciers during the Quaternary²⁶ (see Methods Summary, Supplementary Information, and Supplementary Videos 1 and 2). Modelled glaciers develop as a result of steady cooling over a period of 50 thousand years (kyr) followed by a 50-kyr steady temperature increase. The snowline altitude, which in our model is a linear function of surface temperature, is for both catchments lowered from 2,800 m down to 1,900 m (Fig. 1a, b). This snowline span of 900 m corresponds roughly to the difference between present-day snowline altitudes and suggested Last Glacial Maximum (LGM) snowline altitudes²⁷. Importantly, although it is representative of the LGM snowline variation in the Bitterroot Range, the snowline interval is not meant to represent the actual LGM snowline lowering for Sierra Nevada, where the real snowline altitude reached only the highest parts of the mountain range during the Quaternary²⁵. Instead, the experiment is designed to highlight the isolated effect of catchment hypsometry on glacial extent by keeping everything else equal. For the same reason, no tectonic uplift or erosion is introduced.

For the fluvial catchment in Sierra Nevada, the ice volume increases with a slightly accelerating rate during snowline lowering as the amount of surface area increases downwards (Fig. 1c, d, Supplementary Video 1). However, for the glacially modified catchment in Bitterroot Range, the relationship between snowline lowering and glacial extent is highly nonlinear. The ice volume increases drastically when the snowline altitude reaches the hypsometric maximum (Fig. 1c, Supplementary Video 2). However, as the snowline altitude subsequently falls below the hypsometric maximum, the rate of change in ice volume decreases to values lower than for the Sierra Nevada catchment (Fig. 1d). So, for a similar climatic forcing, the resulting ice volume (that is, areal extent) is very sensitive to the topographic distribution in the two catchments. The nonlinearity between climate change and glacial extent found for glacially modified landscapes is activated when the snowline altitude varies in proximity to the distinct glacial hypsometric maximum, which would be the case for a climate cooling from the present-day level.

We then examine the transient signal in glacial extent and glacial erosion for a climate forcing similar to what is suggested to have prevailed throughout the last 2 Myr of the Quaternary²⁴ by introducing glaciers and glacial erosion in a simulated fluvial steady-state landscape (Fig. 2a, f, and Supplementary Videos 3 and 4). We reproduce the first-order patterns of the Quaternary climate variations by introducing, first, a phase of symmetric constant-magnitude 40-kyr climate cycles (phase 1), followed by a series of asymmetric 100-kyr climate cycles with increasing amplitude (phase 2), leading to an overall decrease in

¹Department of Earth Science, University of Bergen, Allégaten 41, 5007 Bergen, Norway. ²Department of Geoscience, Aarhus University, Høegh-Guldbergs Gade 2, 8000 Aarhus, Denmark.

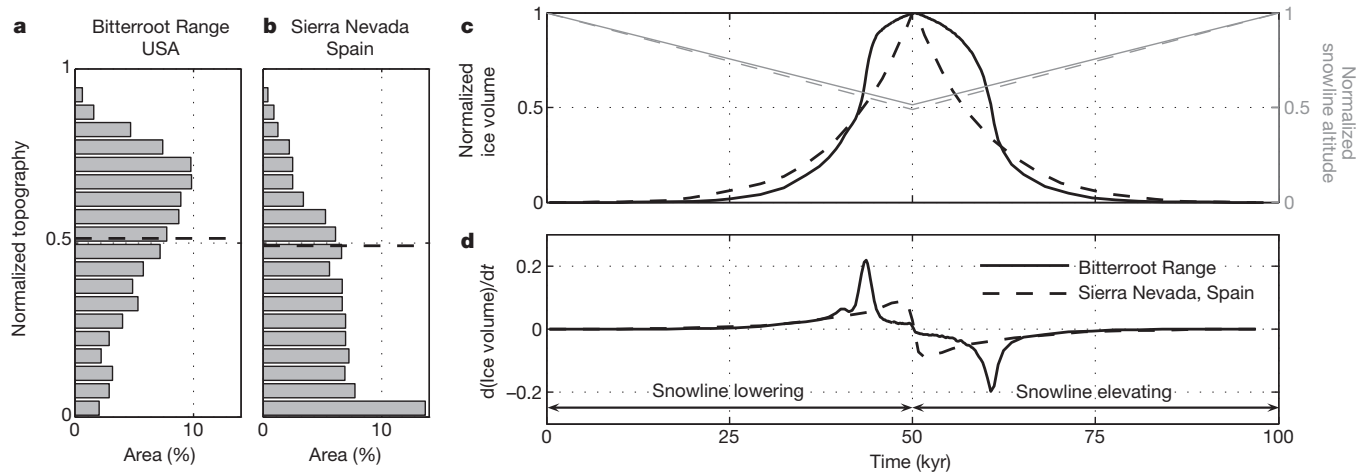


Figure 1 | Ice volume as a function of climate change and hypsometry.

a, b, Hypsometric distributions for the glacially modified Bear Creek catchment in the Bitterroot Range, Montana, USA (46.4° N, 114.4° W), and the fluvial Aldeire catchment from Sierra Nevada, Spain (37.1° N, 3.1° W). The topography has been normalized to the maximum height above the local base level. Black dashed lines represent the minimum level of the snowline altitude at 50 kyr. For a map view see Supplementary Figs 11 and 12. **c**, Temporal

evolution in ice volume for the catchments in Bitterroot Range (solid black line) and in Sierra Nevada (dashed black line) for a changing snowline altitude (solid grey line represents the Bitterroot Range and dashed grey line the Sierra Nevada). **d**, Temporal evolution of the rate of ice volume change for the two landscapes. Animations (Supplementary Video 1 and 2) are available online, showing simulated glaciations in the two catchments.

mean temperature, before a final phase of asymmetric constant-magnitude 100-kyr climate cycles (phase 3, Fig. 2a). To expose the effect of glacial erosion on the areal extent of glaciations, our experiment includes only glacial erosion processes and the resulting flexural isostatic responses of both loading and unloading due to ice and erosion. The change in ice volume (that is, glacial extent) is shown relative to a reference simulation without glacial erosion (Fig. 2b–d).

During the first phase of constant-magnitude climate cycles (Fig. 2a), landforms that are typically associated with a glacial origin emerge. The numerical model includes higher-order ice physics, which facilitates a detailed high-resolution simulation of landscape evolution on scales small enough to resolve U-shaped valleys, hanging valleys, cirques and steep headwalls (Fig. 2h, Supplementary Fig. 14). Furthermore, a hypsometric maximum develops just below the minimum imposed snowline altitude, similar to global observations (Fig. 2e, Supplementary Fig. 1). Concurrently with the development of these topographic features, the ice volume, and therefore glacial erosion, decreases throughout the occurring glaciations as a consequence of glacial erosion, irrespective of climate being constant for each cycle (Figs 2b and 3a). Erosion is, to a high degree, focused in the steep regions above the lowest snowline altitude, where glacial conditions prevail even during the warmest periods of each climate cycle (Fig. 3b). Glacial erosion below the lowest snowline altitude is limited to major valleys, and glaciers reach far below this level only during the coldest periods of the first climate cycles. Thus, glacial erosion lowers mainly the topography at high elevations, reducing the glacier accumulation space and initiating a negative feedback between glacial erosion and glacial extent²⁸.

During the second phase (Fig. 2a) mimicking the mid-Pleistocene transition from 40-kyr to 100-kyr climate cycles, the ice volume increases as a consequence of cooling. More interestingly, the change in ice volume is greater for the glacially modified landscape than for the reference model, and the model with glacial erosion reaches even higher ice volumes than the model without glacial erosion (Fig. 2b, d). In other words, the glaciated cover of the glacially eroded landscape is more sensitive to climatic variations because a lot of surface area is concentrated within a narrow elevation span in the same way as is seen for the Bitterroot catchment compared to the fluvial Sierra Nevada (Fig. 1). Another outcome of focusing surface area within a narrow elevation interval is that the glaciations following glacial erosion initiate later than for the reference model without glacial erosion,

suggesting shorter but more vigorous glaciations in response to the same climatic forcing (Fig. 2b, d). During the constant-magnitude climate cycles in the third phase, the negative feedback between glacial erosion and glacial extent returns, although it is not as pronounced as in phase 1. This is because erosion in phase 1 has already modified the longitudinal and transverse shapes of valleys at high elevations, and these landforms are now associated with smaller subglacial erosion rates than their fluvial counterparts (Supplementary Figs 7 and 15).

As a consequence of the strong negative feedback between glacial erosion, glacial mass balance, and ice extent in phase 1, only limited glacial erosion occurs in the main valley during the constant-magnitude glacial cycles of this phase (Fig. 3a, b). The negative feedback is reflected by the decreasing glacial erosion rate as well as the shorter glacial cycles (Fig. 3a). However, as general cooling is introduced in phase 2, the negative feedback is broken because snowline lowering reincorporates the previously lowered topography into the area available for ice accumulation. This leads to a significant jump in glacial extent across the transition from the ice-poor conditions at the end of phase 1 to the large glaciations in phases 2 and 3 (Fig. 2c), enhancing the potential for glacial erosion in the main valleys (Fig. 3c). The model experiments thus reveal a greater effect of cooling across the mid-Pleistocene transition when the landscape has been prepared by earlier glaciations (Fig. 2c and Supplementary Fig. 28). That the model including glacial erosion has even more ice in phases 2 and 3 than the model without erosion is caused by flexural isostatic rock uplift, adding surface area to the hypsometric maximum from below, in combination with glacially flattened longitudinal valley profiles (Supplementary Figs 15, 17 and 19), which require thicker ice to maintain ice flux from the accumulation zone to the ablation area.

The results presented here thus suggest that topographic modifications occurring throughout the Quaternary may have led to a change in glaciations for the following cycles, by promoting an increasingly nonlinear relation between climate change and the area available for snow and ice accumulation. In particular, as the climate cooled generally throughout the Quaternary, the more extensive glaciations found in the final part of the Quaternary and the contrast in glaciations and glacial erosion across the mid-Pleistocene transition may not only be the direct results of colder temperatures, but also the responses to the developing glacial topographic signature in combination with snowline lowering. The significant increase in simulated glacial extent and glacial erosion across the mid-Pleistocene transition (Figs 2c

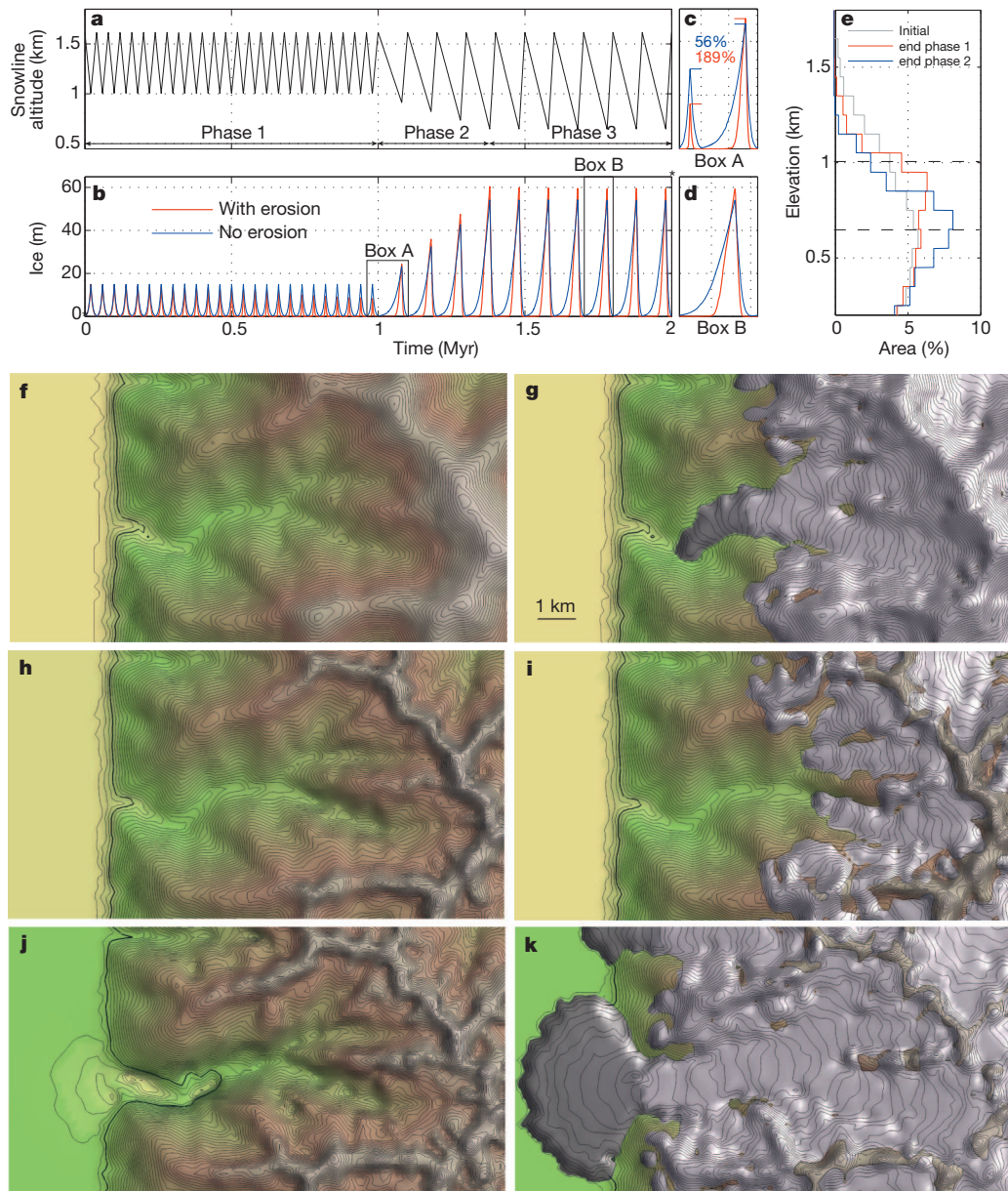


Figure 2 | Transient changes in ice volume for a Quaternary-like climate forcing. **a**, Temporal evolution in snowline altitude. **b**, Temporal evolution in spatially averaged ice volume for models with (red) and without (blue) glacial erosion. For our choice of glacial erosion rate, see experiment S1 in the Supplementary Information. **c**, Enlarged view of the change in ice volume on the transition from phase 1 to phase 2 for the models with (red) and without (blue) glacial erosion, respectively (Box A). **d**, Enlarged view of the glacial cycle in Box B in **b**. **e**, Hypsometric distribution for the initial fluvial landscape (grey), the landscape after phase 1 (red), and the final landscape after phase 3

(blue). The dashed black lines represent the minimum snowline altitude in phases 1 and 3, respectively. **f**, Initial fluvial steady-state landscape. Contour spacing is 25 m. The 100-m contour has been highlighted for reference. **g**, Glacial extent in the first glacial cycle at 20 kyr. **h**, Landscape configuration after phase 1. **i**, Glacial extent in the last glacial cycle of phase 1 at 980 kyr. **j**, Final landscape after phase 3. Note the uplifted foreland caused by flexural isostatic effects. **k**, Glacial extent in the final glacial cycle at 1,980 kyr. Details of modelling parameters, full size figures, and animations are available in the Supplementary Information.

and 3, and Supplementary Fig. 28) can explain results found using exposure dating¹⁰ and low-temperature thermochronology¹¹ in the European Alps, suggesting an increase in relief around a million years ago owing to extensive valley deepening and only minor erosion at higher elevations in association with extensive glaciations following the mid-Pleistocene transition.

In another new study comparing offshore sediment volumes with onshore estimates of fjord erosion in Norway²⁹, it has been suggested that extensive erosion occurred both in fjords and at higher elevations in the Quaternary. This study may therefore record both an initial phase of high-elevation erosion and a subsequent extensive deepening of valleys. By suggesting two different timings of main

cirque formation and main valley deepening, our results therefore reconcile both the hypothesis of bimodal Quaternary glacial erosion^{17,29} and the studies showing an increased relief across the mid-Pleistocene transition^{10,11}.

Climate change is the main driver for glaciations. However, as we have demonstrated here, the topographic distribution that emerges as a result of glacial erosion processes in alpine settings influences the relation between climate and glacial extent in a highly nonlinear manner by changing the area available for snow and ice accumulation. The fact that areas modified recently by glacial erosion processes generally have a distinct hypsometric distribution, with a maximum just below the present day snowline altitude (Supplementary Fig. 1),

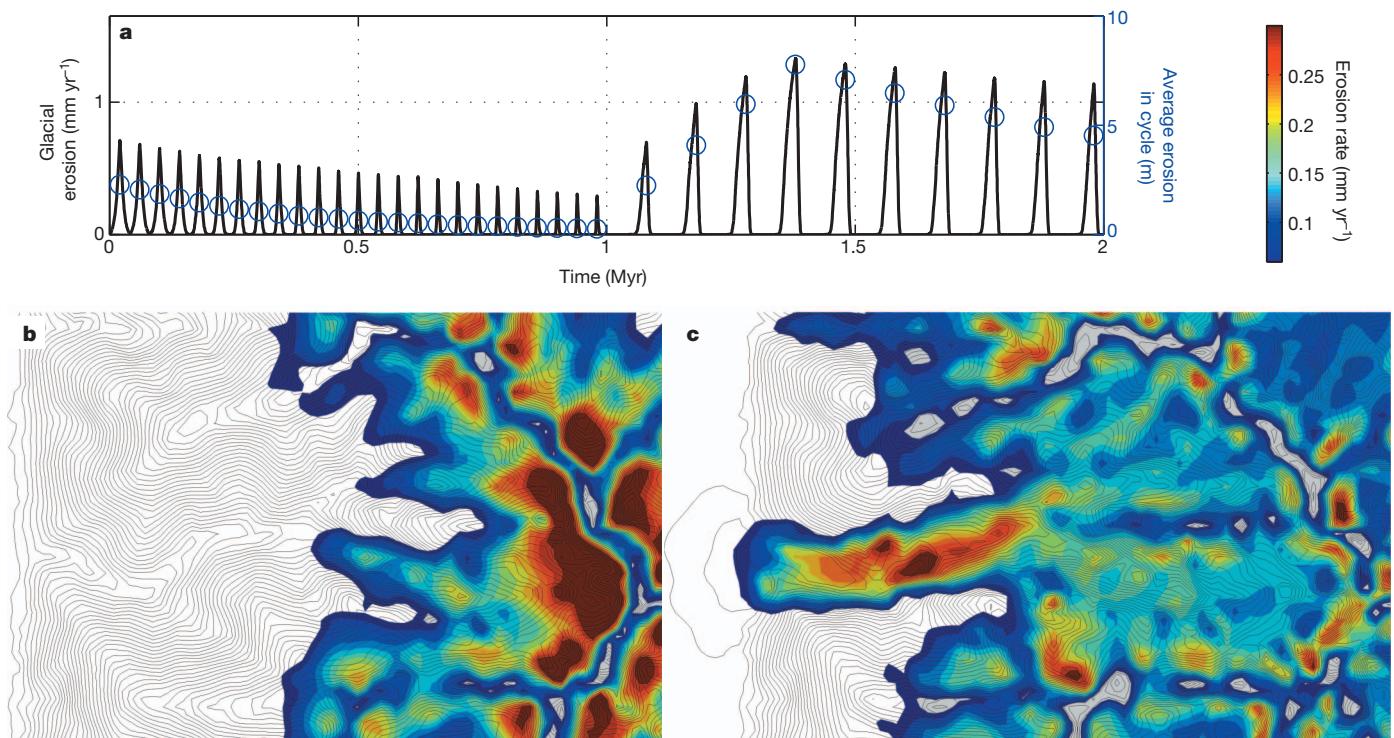


Figure 3 | Variations in glacial erosion for a Quaternary-like climate.

a, Temporal variation in spatially averaged glacial erosion rate (black line) and average glacial erosion for each glacial cycle (blue circles). **b**, Average glacial erosion rate in phase 1. **c**, Average glacial erosion rate in phases 2 and 3. Spatial

glacial erosion patterns are available for representative cycles in Supplementary Figs 24–27. For comparison with glacial erosion rates in the initial fluvial landscape see Supplementary Fig. 28. Erosion histories for representative locations are presented in Supplementary Fig. 29.

suggest that these nonlinear effects may have affected most regions occupied by alpine-type glaciations throughout the Quaternary, and that recent fluctuations in areal extent of glaciations may have been significantly affected by a constantly developing topographic control on glacier mass balance.

METHODS SUMMARY

The numerical surface process model (SPM) we used couples the flow of water, ice and sediment. The flow of ice is handled using a higher-order ice-sheet model, taking into account effects from steep gradients in the bed and ice surfaces, and internal stresses in the ice^{21,22} (integrated Second Order Shallow Ice Approximation; iSOSIA). These effects are of importance when modelling ice flow in alpine settings, and their implementation facilitates detailed predictions of long-term landscape evolution for direct comparison with present-day landforms. On the basis of the flow components, fluvial erosion, glacial erosion (abrasion/quarrying), and mass-wasting processes can be estimated using a set of erosion laws²³. Tectonic uplift and flexural isostatic effects related to loading/unloading of ice and erosion are included. The combined model set-up has been described elsewhere^{21–23}, including testing of the iSOSIA approach against other higher-order ice models as well as full-Stokes solutions for ice flow²¹, however, a summary of the set-up and chosen parameter values can be found in the Supplementary Information.

For the glaciation experiments of real catchments from Sierra Nevada (Spain) and the Bitterroot Range (USA), extracts from the SRTM30 data set were interpolated onto a SPM grid with similar resolution. The experiment illustrating Quaternary evolution (Figs 2 and 3) initiates from a synthetic fluvial steady state, where rock column uplift is balanced by erosion caused by fluvial and hillslope processes. This state is reached by uplifting the model domain (20 km × 20 km) at a constant uniform rate, while fixing the boundary nodes at sea level. The actual experiment excludes tectonic uplift and erosion by fluvial and hillslope processes, except that a local threshold criterion, representing local short-term hillslope processes, prevents the emergence of unrealistic steep surface slopes. Lowland is added to the edge of the model domain in order for ice to extend from the topography.

Received 18 June; accepted 8 November 2012.

1. Brocklehurst, S. H. & Whipple, K. X. Hypsometry of glaciated landscapes. *Earth Surf. Process. Landf.* **29**, 907–926 (2004).

- Egholm, D. L., Nielsen, S. B., Pedersen, V. K. & Lesemann, J. E. Glacial effects limiting mountain height. *Nature* **460**, 884–887 (2009).
- Pedersen, V. K., Egholm, D. L. & Nielsen, S. B. Alpine glacial topography and the rate of rock column uplift: a global perspective. *Geomorphology* **122**, 129–139 (2010).
- Brozović, N., Burbank, D. & Meigs, A. Climatic limits on landscape development in the northwestern Himalaya. *Science* **276**, 571–574 (1997).
- Mitchell, S. G. & Montgomery, D. R. Influence of a glacial buzzsaw on the height and morphology of the Cascade Range in central Washington State, USA. *Quat. Res.* **65**, 96–107 (2006).
- Montgomery, D. R., Balco, G. & Willett, S. D. Climate, tectonics, and the morphology of the Andes. *Geology* **29**, 579–582 (2001).
- Whipple, K. X., Kirby, E. & Brocklehurst, S. H. Geomorphic limits to climate-induced increases in topographic relief. *Nature* **401**, 39–43 (1999).
- Hales, T. C. & Roering, J. J. A frost “buzzsaw” mechanism for erosion of the eastern Southern Alps, New Zealand. *Geomorphology* **107**, 241–253 (2009).
- Delunel, R., van der Beek, P. A., Carcaillet, J., Bourlès, D. L. & Valla, P. G. Frost-cracking control on catchment denudation rates: insights from *in situ* produced ¹⁰Be concentrations in stream sediments (Ecrins–Pelvoux massif, French Western Alps). *Earth Planet. Sci. Lett.* **293**, 72–83 (2010).
- Haeuselmann, P., Granger, D. E., Jeannin, P.-Y. & Lauritzen, S. E. Abrupt glacial valley incision at 0.8 Ma dated from cave deposits in Switzerland. *Geology* **35**, 143–164 (2007).
- Valla, P., Shuster, D. L. & van der Beek, P. A. Significant increase in relief of the European Alps during mid-Pleistocene glaciations. *Nature Geosci.* **4**, 688–692 (2011).
- Kerr, A. Topography, climate and ice masses: a review. *Terra Nova* **5**, 332–342 (1993).
- Oerlemans, J. Numerical experiments on large-scale glacial erosion. *Z. Gletsch. Glazialgeol.* **20**, 107–126 (1984).
- Foster, D., Brocklehurst, S. H. & Gawthorpe, R. L. Glacial-topographic interactions in the Teton Range, Wyoming. *J. Geophys. Res.* **115**, F01007 (2010).
- Brocklehurst, S. H. & Whipple, K. X. Glacial erosion and relief production in the eastern Sierra Nevada, California. *Geomorphology* **42**, 1–24 (2002).
- Braun, J., Zwart, D. & Tomkin, J. A new surface-processes model combining glacial and fluvial erosion. *Ann. Glaciol.* **28**, 282–290 (1999).
- Herman, F., Beaud, F., Champagnac, J.-D., Lemieux, J.-M. & Sternai, P. Glacial hydrology and erosion patterns: a mechanism for carving glacial valleys. *Earth Planet. Sci. Lett.* **310**, 498–508 (2011).
- MacGregor, K., Anderson, R., Anderson, S. & Waddington, E. Numerical simulations of glacial longitudinal profile evolution. *Geology* **28**, 1031–1034 (2000).
- Tomkin, J. Feedbacks and the oscillation of ice masses. *J. Geophys. Res.* **108** (B10), 2488 (2003).

20. Yanites, B. J. & Ehlers, T. A. Global climate and tectonic controls on the denudation of glaciated mountains. *Earth Planet. Sci. Lett.* **325/326**, 63–75 (2012).
21. Egholm, D. L., Knudsen, M. F., Clark, C. D. & Lesemann, J. E. Modeling the flow of glaciers in steep terrains: the integrated Second-Order Shallow Ice Approximation (iSOSIA). *J. Geophys. Res.* **116**, F02012 (2011).
22. Egholm, D. L., Pedersen, V. K., Knudsen, M. F. & Larsen, N. K. On the importance of higher order ice dynamics for glacial landscape evolution. *Geomorphology* **141/142**, 67–80 (2012).
23. Egholm, D. L., Pedersen, V. K., Knudsen, M. F. & Larsen, N. K. Coupling the flow of ice, water, and sediment in a glacial landscape evolution model. *Geomorphology* **141/142**, 47–66 (2012).
24. Lisiecki, L. E. & Raymo, M. E. A. Pliocene-Pleistocene stack of 57 globally distributed benthic $\delta^{18}\text{O}$ records. *Paleoceanography* **20**, PA1003 (2005).
25. Alberti, A. P., Diaz, M. V. & Chao, R. B. in *Quaternary Glaciations—Extent and Chronology. Part I. Europe* (eds Ehlers, J. & Gibbard, P. L.) 389–394 (2004).
26. Weber, W. M. Correlation of Pleistocene glaciation in the Bitterroot Range, Montana, with fluctuations of Glacial Lake Missoula, Montana. *Bur. Mines Geol. Mem.* **42**, 1–44 (1972).
27. Porter, S. C. Some geological implications of average Quaternary glacial conditions. *Quat. Res.* **32**, 245–261 (1989).
28. Kaplan, M. R., Hein, A. S., Hubbard, A. & Lax, S. M. Can glacial erosion limit the extent of glaciation? *Geomorphology* **103**, 172–179 (2009).
29. Steer, P., Huisman, R. S., Valla, P. G., Gac, S. & Herman, F. Bimodal Plio-Quaternary glacial erosion and low-relief surfaces in Scandinavia. *Nature Geosci.* **5**, 635–639 (2012).
30. Farr, T. G. *et al.* The shuttle radar topography mission. *Rev. Geophys.* **45**, RG2004 (2007).

Supplementary Information is available in the online version of the paper.

Acknowledgements V.K.P. thanks the Danish Council for Independent Research and Inge Lehmanns Fund for funding this research. D.L.E. acknowledges funding from the Danish Council for Independent Research under the Sapere Aude Programme. We thank S. Brocklehurst and P. van der Beek for reviews that improved the manuscript considerably.

Author Contributions V.K.P. and D.L.E. performed the global topographic analysis. D.L.E. developed the numerical modelling scheme used. V.K.P. performed the modelling. Both authors contributed equally to the design of the study and writing of the paper.

Author Information Reprints and permissions information is available at www.nature.com/reprints. The authors declare no competing financial interests. Readers are welcome to comment on the online version of the paper. Correspondence and requests for materials should be addressed to V.K.P. (vivi.pedersen@geo.uib.no).